NJC

ROYAL SOCIETY OF CHEMISTRY

PAPER

View Article Online
View Journal | View Issue

Check for updates

Cite this: *New J. Chem.*, 2024, **48**, 16177

Vanadium uptake and storage in the fabrication and function of mussel byssus†

Samantha Jee, Mostafa Rammal, Tobias Priemel, D. Scott Bohle and Matthew J. Harrington *

Mussel byssus is an important model for bio-inspired design, due to the discovery that byssus proteins enriched in the non-canonical amino acid 3,4-dihydroxyphenylalanine (DOPA) form dynamic, load-bearing metal coordination cross-links. While it was initially assumed that cross-linking was based on DOPA–Fe coordination, recent findings challenge this assumption, suggesting that mussels preferentially utilize vanadium. Yet, the details are still unclear. Here, we performed a cross-disciplinary investigation of vanadium use by mussels for formation and function of the byssus, harnessing Raman and X-ray absorption spectroscopy, DFT modeling, and rheological studies. Our results indicate that Mytilus mussels actively uptake vanadium for the express purpose of incorporating it into the byssus, and that byssus V content is influenced by local seawater vanadium concentration. The vanadium oxidation state in the byssus appears to be a mixture of V(IV) and V(III), while the dominant coordination geometry is octahedral tris–DOPA–V. Rheological studies on model DOPA-enriched polymer hydrogels demonstrated that vanadium-reinforced gels exhibit more solid-like behavior than iron-reinforced gels at seawater pH, which may explain why mussels prefer vanadium for building their byssus. These findings offer new insights for how vanadium is used in biology, but also offer further inspiration for novel mussel-inspired adhesive, coatings, and supramolecular materials.

Received 1st June 2024,
Accepted 15th August 2024

DOI: 10.1039/d4nj02546f

rsc.li/njc

Published on 16 Phata 2024. Downloaded on 2025-12-06 11:36:09.

Introduction

Over the last two decades, the marine mussel byssus from *Mytilus* sp. (Fig. 1A) has emerged as a biological role model for inspiring novel metallopolymeric materials with advanced functional properties such as self-healing capacity, tunable mechanics, wet adhesion, and high toughness, due to their use of protein–metal coordination bonds as load-bearing cross-links.[1–3] Yet, the presence of transition metals in the byssus has been the object of intense interest for nearly half a century, even before their functional role was known, because Mytilus mussels have been very useful as biomarkers for heavy metal pollution in marine environments.[4–6] Indeed, a wide range of transition metals, post-transition metals, and even some lanthanides have been found in the soft tissues, shells, and especially, the byssus of these mussels.[6–10] Among these metals are Fe, Ni, Cu, and Cr, as well as Pb and U, and—most relevant to this study—vanadium.[9,11–13] In fact, several pieces of recent evidence suggest that mussels may have a preference for using vanadium for cross-linking purposes in both the adhesive plaque and the protective outer cuticle (Fig. 1B). In both cases, there is convincing spectroscopic evidence that proteins enriched in the rare post-translationally modified amino acid 3,4-dihydroxyphenylalanine (DOPA) forms metal coordination complexes with vanadium, providing mechanical integrity to the byssus.[14–16] Yet, there are still many open questions surrounding the nature of these metal coordination complexes and the process by which they are formed. Here we perform a deep analysis of the vanadium in the byssus.

Mussels are filter feeders capable of ingesting both solubilized and particulate forms of metals from ambient seawater.[17] Once taken up, these metals are metabolized by various soft tissues and often added to the byssus. Previously, it was hypothesized that this pathway was a means of detoxification by which the mussel removed nonessential and toxic metals from the body[8]—a sort of waste disposal system. However, in recent years, it has become abundantly clear that certain transition metals, including iron, zinc, and surprisingly vanadium, influence the assembly and mechanical function of the byssal threads.[15,18–20] Yet, up to this point, there has been very little clear evidence on how specific metals come to be there. In particular, it has been challenging to determine whether this occurs passively through diffusion from seawater, whether this is an active process in which metals first pass

Department of Chemistry, McGill University, 801 Sherbrooke Street West, Montreal, Quebec H3A 0B8, Canada. E-mail: matt.harrington@mcgill.ca

† Electronic supplementary information (ESI) available. See DOI: https://doi.org/10.1039/d4nj02546f

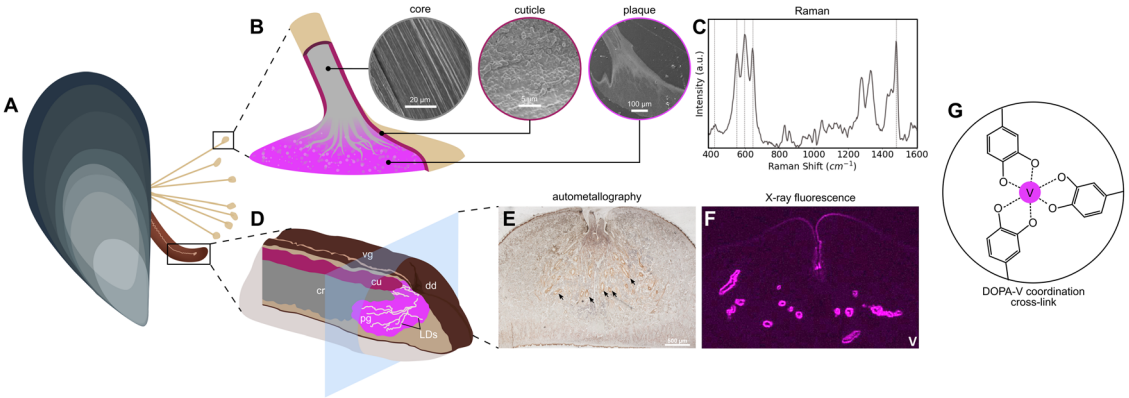

Fig. 1 Vanadium in the formation and function of the mussel byssus. (A) Schematic of a blue mussel (*M. edulis*) showing its byssus and foot, the organ responsible for byssal thread production. (B) Magnified schematic of the distal end of a byssal thread, showing the microstructure of the core, cuticle, and plaque in corresponding SEM images. Regions where vanadium has been identified are highlighted (cuticle, plaque). (C) Raman spectrum showing the characteristic resonance signal of DOPA–metal coordination found in the cuticle and plaque. Resonant Raman peaks are highlighted. (D) Magnified schematic of the mussel foot, showing the secretory glands responsible for production of corresponding regions of the byssal thread. Vg = ventral groove, cr = core gland, cu = cuticle gland, pg = plaque gland, dd = distal depression, LDs = longitudinal ducts. (E) Autometallography stain of a mussel foot cross-section. Positive staining is clear from dark brown/black coloration around the ventral groove and in orange around the LDs (arrowheads). (F) Vanadium μ-X-ray fluorescence image of a mussel foot cross-section. Signal for vanadium is particularly strong around the LDs, though there is some present around the ventral groove as well. (G) Schematic of a tris–DOPA–V coordination cross-link.

Published on 16 Phata 2024. Downloaded on 2025-12-06 11:36:09.

through the soft tissue of the mussel prior to deposition in the byssus, or whether there is a combination of both pathways. Supporting passive uptake, it was previously possible to add metals to metal depleted byssal threads by soaking them in metal chloride solution.[2,3] Yet it was also observed that iron-59 from ^{59}Fe-labelled ferric hydroxide added to aquarium seawater was first incorporated into the mussels' soft tissues and then over a period of several days was measured at high concentration in the byssus, indicating an active uptake mechanism.[8] Further supporting an active incorporation mechanism, very recent work has indicated both iron and vanadium are stored in the mussel secretory organ—the foot—in the form of nanoscale metal storage particles (MSPs) (Fig. 1D–F).[14] In particular, the MSPs are stored in the foot tissue around a network of microchannels known as longitudinal ducts (LDs) in which the plaque proteins are secreted and mixed with the MSPs, leading to curing of the underwater glue *via* formation of DOPA–metal cross-links (Fig. 1D–F).[14]

Given the fact that only a handful of organisms including ascidians, a single species of mushroom and certain species of marine polychaetes are known to hyperaccumulate vanadium for biological functions,[21–23] the discovery of active vanadium accumulation by mussels was particularly striking. In this study we further investigate the uptake and use of vanadium by mussels to form their byssus using a cross-disciplinary approach combining Raman and X-ray absorption spectroscopy, DFT calculations, and rheological studies. Our findings provide clear evidence for the presence and role of tris–DOPA–V complexes in the formation and mechanical function of the mussel byssus and suggest that vanadium may provide superior mechanics under seawater conditions when compared to iron coordination. These findings have clear relevance to understanding the use of vanadium by biological organisms, but also for ongoing efforts to create mussel-inspired adhesives, coatings, and supramolecular materials.[24,25]

Results and discussion

Analysis of DOPA–metal Raman peaks

Raman spectroscopy has provided a convenient means for identifying DOPA–metal complexes in various biological and non-biological systems due to numerous characteristic strong resonance peaks arising from the metal complex.[1,2,26] Notably, previous studies utilizing Raman spectroscopy to measure samples containing DOPA–Fe and DOPA–V complexes have shown differences in the positions of the characteristic resonance Raman peaks between the two metals[1,27]—yet there has not been a systematic analysis of these different studies. Table 1 summarizes a detailed analysis of DOPA–metal Raman spectra from previous literature and current measurements, focusing on the most prominent resonance peaks of interest (Fig. 2). While byssal thread spectra may include contributions of multiple metal complexes, standards using DOPA-modified recombinant mussel byssus proteins and synthetic PEG–DOPA polymers mixed with iron and vanadium provide an opportunity for clearly assigning the peak shifts. Regardless, the most prominent peaks that show clear metal dependent shifts include previously assigned "chelate" peaks at ~530 cm^{-1} (Fe) *vs.* ~550 cm^{-1} (V) and previously unassigned peaks at ~330 cm^{-1} (Fe) and ~418 cm^{-1} (V), as well as a strong peaks for catechol ring vibrations at ~1470 cm^{-1} (V) and ~1480 cm^{-1} (Fe), respectively. Notably, comparison of these control samples with native byssal threads from multiple species from several different water bodies show a clear similarity to the DOPA–V coordination standards and only show

 This journal is © The Royal Society of Chemistry and the Centre National de la Recherche Scientifique 2024

Published on 16 Phata 2024. Downloaded on 2025-12-06 11:36:09.

Table 1 Resonance Raman peak positions of byssal threads from different mussel species, *in vitro* recombinant proteins, and hydrogel standards

			Raman shift (cm^{-1})					
Species/category	Location	Sample	*a*	*b*	*c*	*d*	*e*	Ref.
M. edulis	PEI, Canada	Native cuticle	414	545	600	638	1476	This work
M. galloprovincialis	Italy	Native cuticle	421	550	605	633	1475	This work
M. californianus	California, USA	Native cuticle	418	550	598	637	1479	This work
		Cuticle Fe recovery	315	542	590	633	1482	Harrington 2010[2]
		Cuticle V recovery	418	547	599	630	1472	Schmitt 2015[1]
M. edulis plaque gland + MCl_3	PEI, Canada	$FeCl_3$	337	543	588	637	1482	Priemel 2020[28]
		VCl_3	416	546	596	637	1477	
rMfp-1-DOPA standards		rMfp-1-DOPA–Fe		530	587	634	1487	Mesko 2021[16]
		rMfp-1-DOPA–V^{III}	414	548	597	640	1479	
		rMfp-1-DOPA–$V^{IV}O$	417	547	598	641	1479	
Hydrogel standards		PEG–DOPA–Fe	321	532	564	631	1484	Holten-Andersen 2014[27]
		PEG–DOPA–V	422	551	603	642	1477	

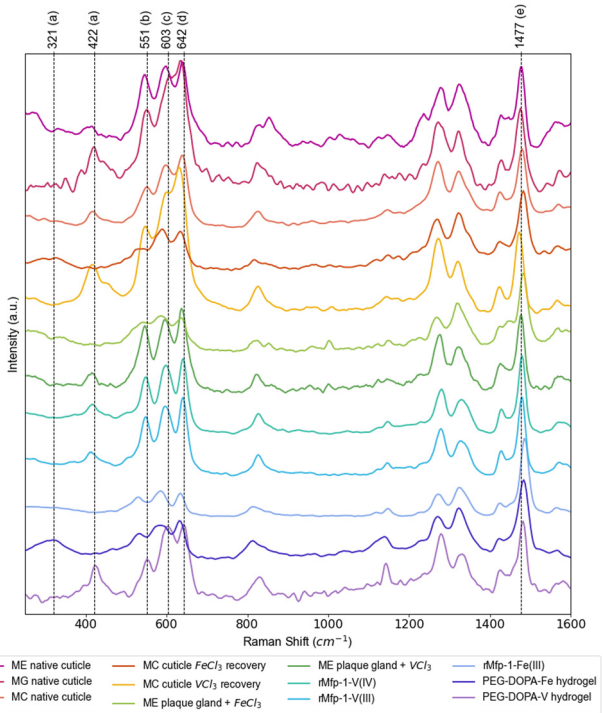

Fig. 2 Raman spectra of DOPA–metal coordination in various *Mytilus* byssus samples and protein/polymer standards. Further examples of Raman spectra acquired from native threads from various Mytilus species acquired from different bodies of water, as well as spectra acquired from plaque gland tissue treated with VCl_3 and $FeCl_3$ solutions and *in vitro* standards. Major resonance Raman peaks for DOPA–metal coordination are labeled a–e as indicated in Table 1. Spectra have been normalized to the resonant peak at ~1480 cm^{-1}, showing the lower relative resonance of the DOPA–Fe peaks in the 500–700 cm^{-1} range. Values for resonance peaks highlighted here (dashed lines) are based on the values taken predominantly from the spectrum for the PEG–DOPA–V hydrogel standard, with the peak at ~330 cm^{-1} taken from the spectrum of the PEG–DOPA–Fe standard. ME = *Mytilus edulis*, MG = *Mytilus galloprovincialis*, MC = *Mytilus californianus*, rMFP-1 = recombinant mussel foot protein-1.

similar to DOPA–Fe spectra when iron is artificially added to metal-depleted threads. The fact that mussel threads from three different species collected around the globe exhibit a clear Raman signal for tris–DOPA–V coordination indicates that this is not due to local elevation of vanadium in polluted waters, but rather suggests that mussels preferentially accumulate vanadium for use in the byssus over other metals.

Single particle Raman analysis of MSPs

While the signal of DOPA–V coordination was clearly seen across species and locations in the native byssus fibers, we are interested here in the origin of the vanadium that ends up in the threads—*i.e.* how it is acquired and subsequently stored by the mussel. In order to investigate this, we turn our attention to the MSPs surrounding the longitudinal ducts (LDs) in the mussel foot (Fig. 1F), which is where the mussel stores the vanadium that eventually becomes incorporated into the thread plaque. Previously, only averaged spectra surrounding the LDs was reported.[14] Here, we perform high-resolution (~300 nm) confocal Raman spectroscopic mapping to extract resonance Raman spectra from individual MSPs, which enabled us to examine the variability in the positions of the Raman peaks, providing insights into variations in the metals complexed and their local coordination environment. Notably, the coordination complexes in the MSPs seem to vary only slightly from particle to particle, since peak position and shape of the resonance Raman bands are at first glance largely similar between different MSPs (Fig. 3C–E). The small amount of variation observed may indicate some variation in the identity of the coordinated metal, differences in coordination bond length or slight variations in coordination geometry;[29] however, the overall similarity from particle to particle is clear. Indeed, the storage of mixtures of vanadium and iron in different ratios may partially explain the peak position diversity, which is also consistent with previous spectroscopic findings of individual MSPs using TEM-EDX showing that both metals are co-localized in single MSPs.[14] This is also consistent with previous reports that

Published on 16 Phata 2024. Downloaded on 2025-12-06 11:36:09.

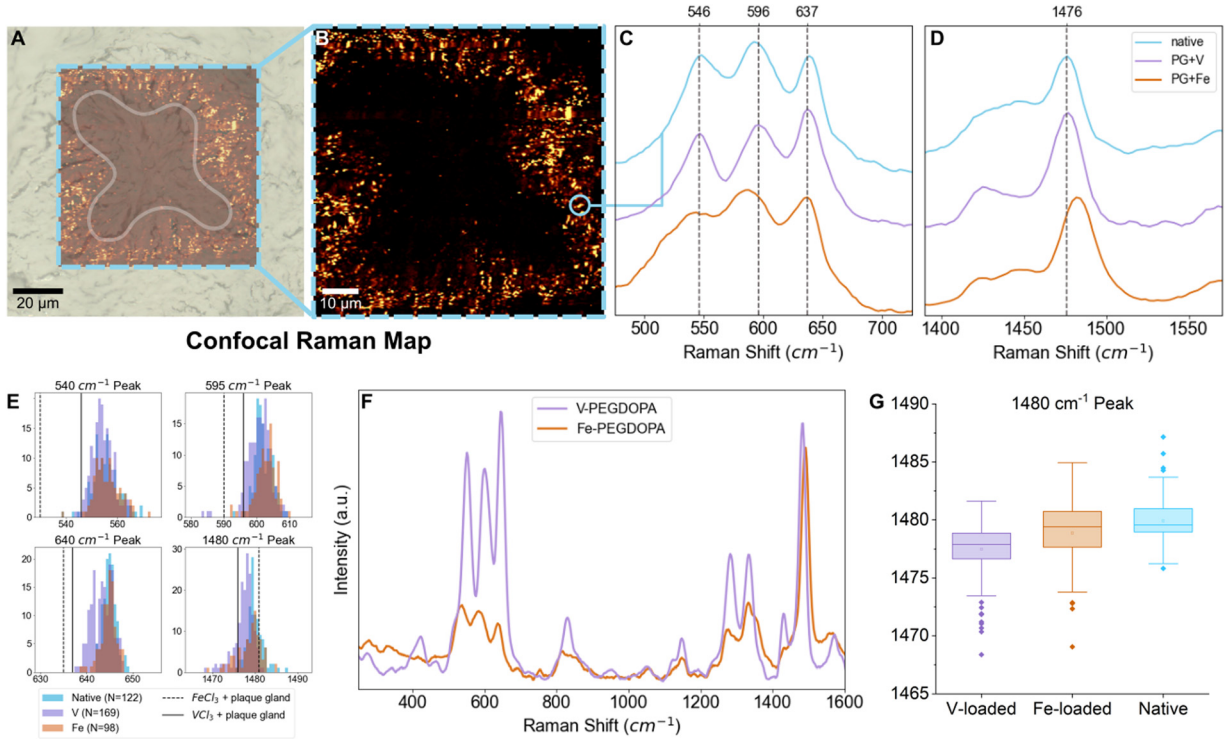

Fig. 3 Statistical analysis of individual MSP resonance Raman spectra following metal-loading experiments. (A) and (B) Raman spectroscopic map of a longitudinal duct cross-section. The shape of the LD cross-section is highlighted in (A); only a portion of the LD was measured, and the resulting map shown in (B) shows the distribution of spectra characteristic of MSPs. (C) and (D) Example resonance Raman signals acquired from an individual MSP taken from the Raman map in (B) (shown in light purple) compared to spectra of plaque gland tissue with added $FeCl_3$ (bottom) or VCl_3 (middle) solution. (E) Histograms of different resonant peaks with populations from vanadium-exposed (purple), iron-exposed (orange), or native (blue) mussels. (F) Raman spectra of PEG–DOPA–V (purple) and PEG–DOPA–Fe (orange) hydrogel standards at 532 nm, normalized to the non-resonant C–H stretch at $\sim$2880 cm^{-1}. (G) Box plot showing the distribution of peak positions of the resonant signal at $\sim$1480 cm^{-1} for vanadium-exposed (purple), iron-exposed (orange), and native (blue) mussels.

mussels are typically opportunistic in their accumulation of metals that are used to fortify the byssus and are dependent on what is available in their local environment.[1] Nonetheless, the positions of the peaks appear to show a clear predominance of vanadium, when compared to iron and vanadium standards (Table 1 and Fig. 3C). It is important to mention that these are resonant Raman modes and therefore the intensity might not necessarily reflect the true relative amount of the two metals. Complicating this analysis is the fact that the relative degree of resonance enhancement at a specific wavelength is dependent on the absorbance behavior of the different metal complexes, as shown from studies on PEG–DOPA–metal standards (Fig. 3F). Notably, however, the relative intensities of the resonance peaks at $\sim$1470 cm^{-1} (V) and $\sim$1480 cm^{-1} (Fe) compared to non-resonant polymer peaks are quite comparable when using the 532 nm green laser employed in this study. Thus, using this specific peak as a rough approximation for presence of iron and vanadium presence seems reasonable. In any case, the presence of vanadium coordination is indisputable even if we cannot quantify the relative amounts of coordinated vanadium *vs.* iron.

Metal loading experiments

To demonstrate that the metal content of the local environment in which the mussels live has an effect on the metal composition of the MSPs, we carried out metal loading experiments on aquaria seawater. Following existing protocols,[30] mussels were exposed for one day to high concentration of particulate vanadium or iron and then were placed in an aquarium containing regular seawater for three days before dissection. Micron-sized particulate metal (iron, vanadium) species were selected for seawater loading with the intention of not changing physicochemical properties of the seawater such as pH or ionic strength, or adding other counterions from various soluble metal salts that could otherwise affect the uptake of metals. Previous studies demonstrated that exposing mussels to varying concentrations of particulate iron for 24 hours affected the adhesive performance of the byssal threads produced thereafter, indicating that three days should be sufficient time for the mussels to metabolize metals into the byssus.[30] Metal storage was characterized in the LDs using autometallography staining (AMG), confocal Raman spectroscopy, and inductively coupled plasma mass spectrometry (ICP-MS). Focusing on the position of the resonance Raman peak arising from the DOPA ring vibration (1470–1480 cm^{-1})[26] in which DOPA–Fe and DOPA–V resonance is comparable at an excitation wavelength of 532 nm, MSPs from vanadium-exposed mussels showed a small but clear shift toward lower wavenumbers consistent with the PEG–DOPA–V control (Table 1). However, the average peak maximum is still not as low

 This journal is © The Royal Society of Chemistry and the Centre National de la Recherche Scientifique 2024

Published on 16 Phata 2024. Downloaded on 2025-12-06 11:36:09.

Table 2 ANOVA table for metal-loading experiments

		540		590		640		1480	
Group	*N*	Mean (cm^{-1})	Std dev. (cm^{-1})	Mean (cm^{-1})	Std dev. (cm^{-1})	Mean (cm^{-1})	Std dev. (cm^{-1})	Mean (cm^{-1})	Std dev. (cm^{-1})
V-exposed	169	554.29	4.08	600.69	3.66	643.43	2.22	1477.48	2.21
Fe-exposed	97	556.05	5.05	602.64	3.20	644.75	1.73	1478.87	2.77
Native	122	555.51	5.61	602.01	2.56	644.98	1.34	1479.91	1.88
α		0.05		0.05		0.05		0.05	
F value		4.67		12.77		29.34		41.65	
p value		0.0099		<0.0001		<0.0001		<0.0001	

as the PEG–DOPA–V standard, suggesting there is still a mixture of Fe, V and possibly other metals within the MSPs (Table 2).

Using spectra from individual MSPs from native, iron-exposed, and vanadium-exposed mussels, the Raman shift variance of characteristic resonant peaks was examined using one-way analysis of variance (ANOVA), with the null hypothesis rejected when $p < 0.05$. For the DOPA ring vibration at $\sim$1480 cm^{-1}, the ANOVA *F* value was 41.65, with a *p* value of <0.0001 (Table 2). A Tukey *post hoc* test was also performed to check for statistically significant differences between datasets (native, V-exposed, and Fe-exposed mussels) at this confidence interval and found that for this resonant peak, each pair of datasets was significantly different from each other, consistent with a compositional change in the MSPs under different loading conditions (Fig. 3G and Table 2). The other resonance peaks also show statistically significant shifts in peak positions in the vanadium-exposed mussels. However, there is a much stronger resonance enhancement of these peaks for DOPA–V *vs.* DOPA–Fe at the excitation wavelength of 532 nm. Notably, in all cases, the resonant peak positions of the spectra acquired from MSPs in the iron-exposed mussels is more similar to the native MSPs than those from the V-exposed mussels (Tables S1–S4 and Fig. S1, ESI†).

Consistent with these spectroscopic findings, ICP-MS experiments on the foot and whole byssus showed an increase in vanadium concentration in byssal threads from vanadium-exposed mussels relative to native mussels (Table 3). Moreover, the iron present in the byssus seems to decrease in vanadium-exposed mussels, suggesting its replacement by vanadium and supporting the opportunistic behaviour in metal bioaccumulation by mussels. Notably, zinc levels in both the byssus and foot remain relatively constant within error between metal loading and native conditions. This makes sense given its distinct His-based coordination environment[18] and placement in the core of the byssus rather than the cuticle, and suggests similar uptake mechanisms for iron and vanadium. It should be noted, however, that previous studies showed that iron present in the cuticle was preferentially associated with the sulfur-rich matrix, while vanadium was associated with the DOPA-rich granules.[15] This indicates that not all the Fe detected through ICP-MS is interacting with DOPA. Overall, these results provide clear evidence that mussels can actively incorporate vanadium into their tissues through uptake of particulate matter expressly for the purpose of producing byssal threads.

DFT analysis

Our investigation clearly shows that DOPA–V and DOPA–Fe coordination results in different resonance Raman spectral signatures. However, there is still some uncertainty of the vibrational modes to which these characteristic Raman peaks correspond. Indeed, there have been some studies that have attempted to assign the vibrational modes through the use of heavy oxygen isotopes, but they do not paint a complete picture of the likely complex vibrational modes present and importantly, have not provided a good explanation for the unassigned peaks at lower wavenumbers, which appear at $\sim$330 cm^{-1} for iron and $\sim$420 cm^{-1} for vanadium. Considering how prevalent the use of resonance Raman for identifying DOPA–metal coordination is in the literature, it is important to better understand these peaks and the vibrational modes which give rise to them. Thus, we performed here density functional theory (DFT) calculations of iron tris–catecholate and vanadium tris–catecholate, as these are the most likely species present based on previous studies.[16]

DFT analysis of different metal DOPA–Fe and DOPA–V complexes allows us to assign some of these specific Raman peaks to characteristic vibrational modes that are specific to the different metal complexes (Tables S5 and S6, ESI†). According to DFT, the vibrational modes are complex, for example incorporating C–H bending strongly into metal–ligand deformation or stretching modes, and not quite as simple as previously proposed through studies using model catechols with heavy oxygen atoms substituted in the 3 and 4 positions of the catechol ring.[26] DFT was particularly useful in the assignment of the low energy metal–oxygen vibrational modes at 330 cm^{-1}

Table 3 Metal concentrations of the byssus and mussel foot of V-exposed and native *M. edulis* by ICP-MS

Sample	Group	V ($\mu g\ g^{-1}$)	Fe ($\mu g\ g^{-1}$)	Zn ($\mu g\ g^{-1}$)
Byssus	V-exposed	64.61 ± 7.92	90.77 ± 1.45	409.27 ± 15.73
	Native	31.51 ± 14.62	193.69 ± 10.13	513.77 ± 81.97
Mussel foot	V-exposed	1.69 ± 1.24	62. 13 ± 7.46	63.98 ± 14.81
	Native	0.44 ± 0.27	96.19 ± 45.81	58.72 ± 3.36

Published on 16 Phata 2024. Downloaded on 2025-12-06 11:36:09.

Table 4 Calculated frequencies of metal–tris–catecholate complexes with high Raman activity[a]

Metal-dependent catecholate vibrational modes			
		$[V(cat)_3]^{2-}$	$[Fe(cat)_3]^{3-}$
Description	Mode (for $[V(cat)_3]^{2-}$ complex)	Frequency (cm^{-1})	Frequency (cm^{-1})
Metal–oxygen mode	20	420.49	331.04
Catechol scissors	25	509.62	477.03
	26	509.68	477.05
Catechol rocking	29	546.27	498
Asymmetric ν(C–O–M)	37	631.81	599.56
	38	631.84	599.59
Symmetric ν(C–O–M)	39	634.15	604.17
	48	820.55	785.54
Symmetric catechol ring mode	73	1294.27	1302.38
	74	1294.28	1302.42
	78	1314.41	1321.04
Catechol breathing mode	79	1374.28	1357.54
	80	1374.31	1357.58
Symmetric catechol ring mode	81	1375.64	1359.9
	85	1502.51	1515.37
	86	1502.55	1515.38
	88	1580.35	1549.34
	89	1580.36	1549.35

[a] These bands all have strong Raman activity. Bands 25, 26, 37, 38, 73, and 74 also have strong IR activity.

and 420 cm^{-1} for DOPA–Fe and DOPA–V, respectively (Table 4), which had previously never been assigned, but which provide the largest change in position ($\sim$90 cm^{-1}) of all the resonance peaks. The assignments possible through DFT analysis establishes clear vibrational indicators for the presence of vanadium *vs.* iron and provides a useful Raman-based assay for confocally mapping the movement of metal complexes during uptake and storage in the mussel tissue and in the byssus. However, it is important to recognize that the relative intensity of the metal–tris–catecholate resonance Raman signals from different DOPA–metal complexes will depend on the wavelength of the laser excitation.

EXAFS analysis of metal coordination environment

While Raman spectroscopic analysis and DFT analysis provide important insights into the nature of the DOPA–V coordination bonds present in the byssal threads and MSPs, more detailed information about the complexes including oxidation state, coordination number, and first-shell bond lengths and geometries requires more advanced methodologies. To investigate these aspects of the V complexes in the byssus, we utilized X-ray absorption spectroscopy (XAS) with X-ray absorption near-edge spectroscopy (XANES) and extended-edge X-ray absorption fine structure (EXAFS) analysis (Fig. 4). Comparison of the edge energies (taken as the maximum of the first derivative in energy space) of the byssal cuticle and plaque with vanadium oxide standards from the International X-ray Absorption Society online database[31] in the +(III), +(IV), and +(V) oxidation states indicates that the vanadium species present in the byssus are a mixture of +(III) and +(IV).[32] It is difficult to quantify exactly how much of each oxidation state is present without performing linear combination fitting with more structurally similar standards. However, this finding is consistent with previous EPR and UV-vis investigations[16] and indicates that vanadium undergoes a reduction during its uptake and metabolism by the mussel, since it exists predominantly as the V(v) vanadate anion, $[VO_4]^{3-}$, in seawater,[33] but then is reduced either during compartmentalization or byssal thread formation. The best first shell (*R*-range of 1–2.6 Å) fitting results were obtained using an octahedral model of six equidistant oxygen neighbours. The resulting bond lengths of 1.99 Å and 1.97 Å for the byssal cuticle and plaque respectively (Table 5) are consistent with the bond lengths predicted for a vanadium–tris–catecholate by DFT simulation, which were found to be 1.96 Å on average. It is worth noting that the quality of the data at higher k is limited by the biological nature of the sample and low concentrations of analyte metal. A Fourier transform range of 2–8 Å and a fitting range of 1–2.6 Å allows for the extraction of five independent data points.[34,35] These restrictions, while still sufficient for first-shell fitting, result in a simplified depiction of the true structure present; it is unlikely that the native coordination complex is perfectly octahedral, since the presence of the pre-edge feature in vanadium XANES spectra indicates the presence of 1s $\rightarrow$ 3d electronic transitions that are made possible through lowering of symmetry.[34,35] However, it is also likely that since XAS spectra average the signals from all complexes present under the incident beam, there will be varying degrees of symmetry averaged in the spectra, especially

 This journal is © The Royal Society of Chemistry and the Centre National de la Recherche Scientifique 2024

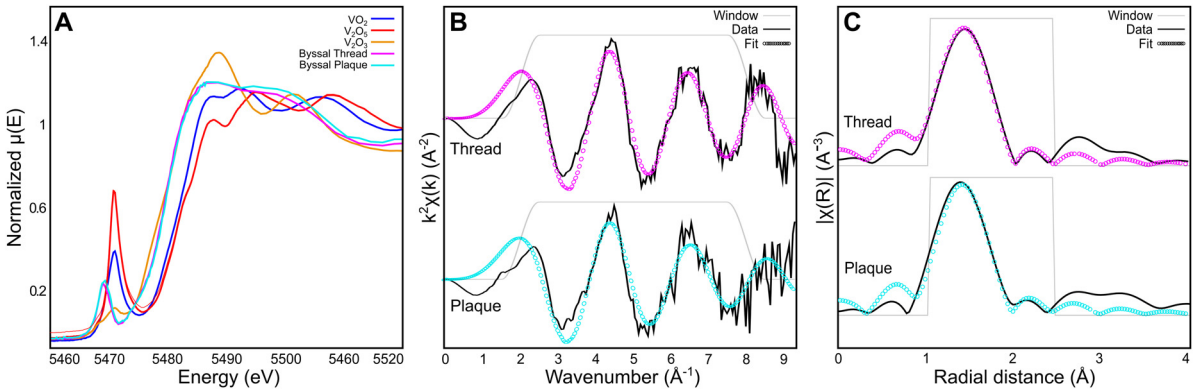

Fig. 4 Vanadium Kα edge XAS analysis of byssal thread cuticle and plaque. (A) Vanadium XANES spectra averaged from the byssal thread cuticle (pink) and plaque (cyan) compared to vanadium oxide standards from the International X-ray Absorption Society online database.[31] (B) Vanadium EXAFS first shell fit from the byssal thread cuticle and plaque shown in *k*-space with a *k*-weight of 2. (C) Vanadium EXAFS first shell fit from the byssal thread and plaque shown in *R*-space with a *k*-weight of 2.

Table 5 Best fit parameters for the first shell EXAFS spectra collected from the cuticle and plaque of *M. edulis* byssal threads (cuticle *N* = 4, plaque *N* = 3)

	Fit parameters				
Region	S_0^2	E_0 (eV)	*R*-factor (%)	First shell bond length (Å)	First shell σ^2 (Debye Waller factor, Å^2)
Cuticle (thread)	0.72	0 (2)	1	1.99 (2)	0.003 (1)
Plaque	0.72	−3 (3)	2.5	1.97 (3)	0.006 (2)

Errors are given in brackets on the last digit. S_0^2 is the amplitude reduction factor, E_0 is the energy shift, the *R*-factor is the fit agreement in percent, and the Debye Waller factor is the mean square relative displacement for the given scattering path.[36,37]

for a biological sample. Nonetheless, these studies provide unequivocal evidence for the presence of highly similar octahedral tris–catechol–V complexes in two compositionally, structurally, and functionally distinct regions of the thread.

DOPA–V *vs.* DOPA–Fe mechanics

Thus far, we have provided clear evidence for the presence of DOPA–V complexes in the MSPs and also the byssal thread cuticle and plaque. Previous spectroscopic imaging studies have indicated that vanadium is co-localized with DOPA in the cuticle rather than iron,[15] while *in vitro* studies of recombinant cuticle proteins showed a strong preference for binding to vanadium, even in the presence of iron.[16] These results naturally raise the intriguing question of why the mussel apparently "prefers" to utilize DOPA–V as opposed to DOPA–Fe in this functional role in spite of the fact that both metals are available to the mussel and essentially equally abundant. To examine this question, we used PEG–DOPA hydrogels as a model system where we can systematically vary the metal crosslink and study its effect on the bulk mechanics.[27] Given that the mussel byssus functions in a seawater pH of 8.2, it is important to perform these comparative mechanical experiments under biologically relevant conditions. At this pH ≈ 8, hydrogels crosslinked using vanadium exhibit lower crossover frequency and slower relaxation time ($\tau_c = 1/\omega_c$) compared to iron cross-linked gels (Fig. 5A). This means that the V-based hydrogels behave more solid-like over a larger range of frequencies than the Fe-based gels, which has relevance for the function of the byssus material in marine environment. Crossover frequency and relaxation time is influenced by the supramolecular bond lifetime of the metal complexes (among other factors), possibly indicating that DOPA–V bonds kinetics are slower than those of the DOPA–Fe bond, which can strengthen the hydrogel network.[38] Essentially, this means that it would be statistically less likely for the DOPA–V bonds to be replaced by Fe as they are less prone to dissociate. This is consistent with previous studies using DOPA-containing mussel proteins.[16] However, this rather simple interpretation assumes an identical network topology and cross-link density[37] between the DOPA–V and DOPA–Fe, which might not be the case and needs to be further examined.

To further investigate the difference in dissociation dynamics, we performed frequency sweep measurements at varying temperatures on both gels (Fig. 5B and C). The relaxation time ($\tau_c = 1/\omega_c$), calculated from the crossover frequency, depends strongly on the temperature and is an important measure for the network relaxation dynamics. In both gels, the crossover frequency shifts to higher values indicating a shorter relaxation time. However, vanadium gels maintained a longer relaxation time at all temperatures (*i.e.*, behaved more solid-like across a wider range of frequencies). The dissociation mechanism of metal crosslinked hydrogels is a thermally activated process,[25] so we can extract the activation energy barrier from the change of relaxation time with respect to temperature using Arrhenius law (Fig. 5D):

$$\ln \tau(T) = \frac{E_a}{kT} + \ln \tau_0$$

Published on 16 Phata 2024. Downloaded on 2025-12-06 11:36:09.

Published on 16 Phata 2024. Downloaded on 2025-12-06 11:36:09.

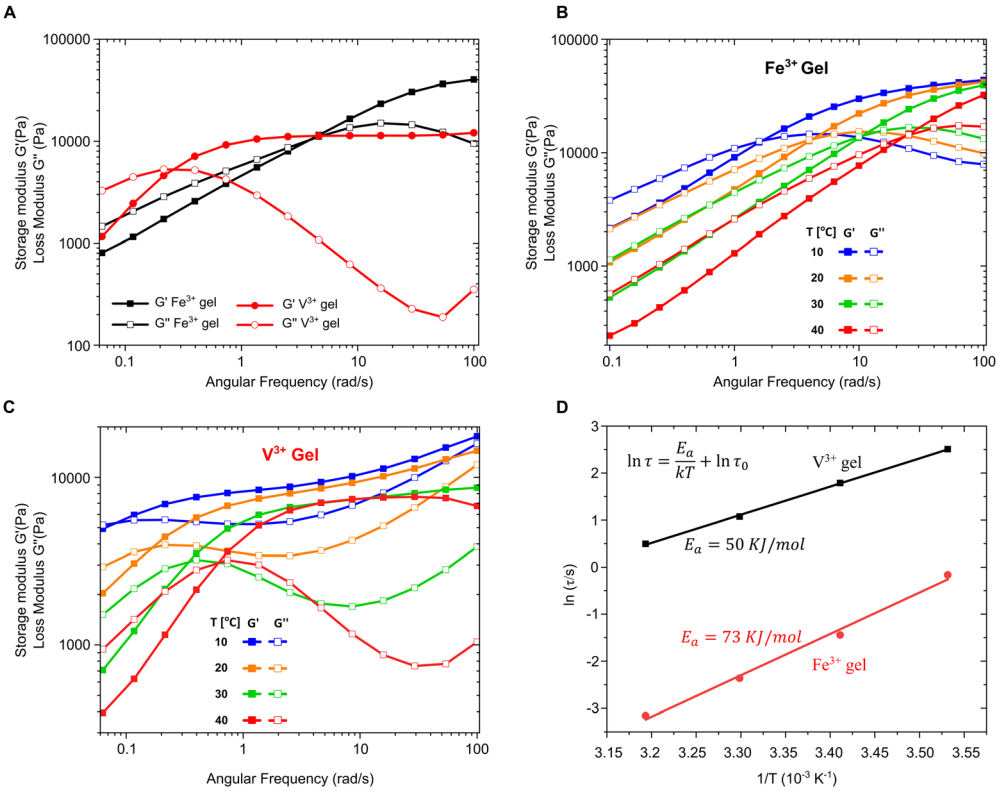

Fig. 5 Rheological analysis of PEG–DOPA–V and PEG–DOPA–V hydrogels. (A) Frequency sweep (1% strain) of Fe^{3+} gel (black) and V^{3+} gel (red) at room temperature. (B) and (C) Frequency sweeps at varying temperatures for Fe^{3+} gel and V^{3+} gel respectively. (D) Relaxation time ($\ln \tau$) *versus* inverse temperature ($1/T$) fitted to an Arrhenius law.

Surprisingly, the activation energy of vanadium-crosslinked gels (50 kJ mol^{-1}) is only two-thirds of that calculated for the iron-crosslinked gels (E_a = 73 kJ mol^{-1}) although the former exhibits a slower relaxation at all the temperatures examined. Although lower activation energy should result in a shorter relaxation time and more dynamic network, it seems that the relaxation of the vanadium–catechol crosslinked networks is also influenced by other factors beyond the bond lifetime, such as differences in cross-link density, network topology, polymer entanglements and most relevant to our current example perhaps, metal complex geometry and coordination number.[39,40] Indeed, the very first investigation of PEG–DOPA–Fe hydrogels[41] demonstrated that at a pH of 8, bis-catecholate coordination of Fe dominates, leading to a loosely crosslinked fast relaxing network, while later studies showed that under these same conditions vanadium will tend to tris–catecholate complexes[27,42] leading to two very different network topologies (*i.e.*, cross-link nodes connecting three *vs.* two polymer chains in DOPA–V *vs.* DOPA–Fe hydrogels, respectively). It is imaginable that this difference in network topology might lead to the vanadium-stabilized networks exhibiting slower relaxation than iron-stabilized networks even if they have a lower E_a. In summary, these results demonstrate that under biologically relevant conditions, vanadium forms a more stable network with DOPA, exhibiting slower relaxation behavior. Thus, considering that these gels were tested under biologically relevant pH conditions, the improved mechanics of DOPA–V might in part explain why mussels appear to utilize vanadium to build the byssus.

Broader context and implications of vanadium use by mussels

The specific uptake and storage of vanadium is highly unusual and reported in exceedingly few cases in nature, most notably in the blood of ascidians.[43,44] Indeed, the mussel's storage and use of vanadium to fabricate an adhesive material is remarkable considering there are only three other examples of organisms known to accumulate vanadium to a significant degree—ascidians, the mushroom species *Amanita muscaria* and some species of seballarid polychaetes.[21–23] Notably, the function of vanadium is not well established in any of these three examples, even after more than 100 years of study in the case of ascidians,[21–23] whereas the current study and others indicate that vanadium is serving a clear mechanical cross-linking function in the byssus cuticle[1,16] and plaque,[14] which has been mimicked successfully in mussel-inspired hydrogels.[27] The most prominent and well-studied example of vanadium hyperaccumulation is in ascidians (a.k.a. tunicates or sea squirts),[21,44,45] which can reach a concentration of up to ~350 mM in the blood of some species, which is 10 million-fold higher than the seawater concentration.[46] This raises the question of how vanadium is specifically concentrated in biology, including by mussels. In seawater, almost all the

 This journal is © The Royal Society of Chemistry and the Centre National de la Recherche Scientifique 2024

Published on 16 Phata 2024. Downloaded on 2025-12-06 11:36:09.

vanadium is present primarily in the monomeric pentavalent ionic form $H_2VO_4^-$, which is similar in structure to a phosphate anion, leading to the proposal that it might be initially acquired by organisms through existing phosphate uptake pathways.[21,47] However, in ascidians, and apparently mussels, this V(v) form is reduced to V(iv) and V(iii), both of which are unstable at physiological pH. To stabilize these oxidation states in ascidians, it was shown that V(iv), present in their cytoplasm, is complexed by a Cys-rich protein known as vanabin *via* interaction with Lys, Arg and His residues,[43,48] which is proposed to function both as a transporter and reducing agent. On the other hand, V(iii) is heavily concentrated and stabilized within small cells in the ascidian blood known as vanadocytes in which the V(iii) is associated with high concentrations of sulfate ions and held at an extremely low pH (0–3), under which the V(iii) form is stabilized.[21,46] In the mushroom *A. muscaria*, hyperaccumulated vanadium ions are stored in the V(iv) oxidation state associated with a small molecule natural product known as amavadin; yet, similar to ascidians, the function of V remains elusive.[21,22,47]

Our findings indicate that the storage of vanadium (and iron) in the MSPs in the mussel foot and complexation in the byssal thread plaque and cuticle is mediated by a different mechanism than that observed in either ascidians or *A. muscaria*. Indeed, in all cases, the metal ions are complexed *via* catechol moieties. While we do not know the nature of the organic molecule or the internal conditions of the MSPs, we infer that the conditions are not acidic due to the presence of the charge transfer peak in the resonance Raman spectrum ($\sim$541 cm^{-1}) indicating bidentate chelation,[26] which is not favored at acidic pH.[27,41] Octahedral coordination appears to dominate in the cuticle and plaque as well. Tunicates also contain a molecule known as tunichrome that contains pyrogallol moieties, structurally and functionally similar to catechols, that are capable of coordinating V ions and reducing V(v) to V(iv); however, it is now accepted that tunichrome and vanadium are stored separately in the ascidian blood and do not interact *in* vivo.[21,22] Similarly, it was shown that the bacterial siderophore enterobactin, which possesses three catechol groups, is able to complex V(iv), although its biological function is to scavenge Fe(iii) in iron-limited marine environments.[49] While the identity of the DOPA-rich proteins in the byssus cuticle and plaque are well characterized,[50] the yet unknown protein present within the MSPs appears to be the first reported instance of DOPA-based molecule functioning to store and transport vanadium, as well as iron, in a biological role *in vivo*. It seems plausible that the vanadium is stored in the V(iv) oxidation state since catechols have been previously shown to reduce V(v) to V(iv) following complexation.[21,51] Consistent with this, V(iv) was previously found to be present in native thread cuticle and plaque materials using EPR,[1,16] which is consistent with our current XANES and EXAFS results.

A final important question concerns why the mussel is using vanadium in the first place – what are the functional advantages? It was recently observed in the mussel byssus cuticle, which provides a hard coating on the byssus fibers, that vanadium is co-localized and coordinated to DOPA-rich proteins in hard submicron granules[15] whereas iron was observed to self-segregate and co-localize with sulfur-rich matrix proteins. It was proposed in this case that this metal self-sorting is a diffusion and competition effect related to the longer bond lifetime (*i.e.* slower dissociation kinetics) of the DOPA–V *vis-a-vis* the DOPA–Fe complexes.[27] Our analysis of the viscoelastic properties of hydrogels based on DOPA–V *vs.* DOPA–Fe cross-linking suggest that the reason might be more complex and related to the different bond topologies existing in vanadium *vs.* iron cross-linked protein networks under seawater pH of 8.2 under which previous studies have shown that vanadium will tend toward tris coordination whereas iron will tend toward bis coordination.[41] Analogously, metal storage by the mussels in the MSPs using a DOPA-based protein[14] may have a natural preference to concentrate vanadium over iron, although the exact mix of metals may depend strongly on the local water chemistry as we have seen. Indeed, there is evidence that mussels are opportunistic regarding which metal ions they acquire and utilize to construct their byssus depending on the local composition of the seawater.[1,7,30] Nonetheless, our reassessment of resonance Raman signals from earlier studies, suggests that DOPA–V coordination is a common feature as observed in the byssal threads of at least three different mussel species from the *Mytilus* genus acquired from very different bodies of water including the coast of California, the Mediterranean Sea and the Atlantic Ocean off the eastern coast of Canada (Table 1 and Fig. 2).[1,2,16,27] This indicates a clear preference by mussels to use vanadium to build their threads, which might suggest that materials researchers who are inspired by the mussel should explore the potential benefits of switching from iron to vanadium coordination.

Conclusions

The findings of this study and previous investigations clearly reveal that mussels actively accumulate vanadium and complex it with an unknown DOPA-rich storage protein within submicron metal storage particles (MSPs) in the mussel foot tissue. During thread formation, the vanadium in the MSPs is incorporated into the byssus creating mechanically important cross-links. This seems to be a consistent observation across at least three different species of Mytilus mussels from around the world. These findings have important implications for the understanding of transition metal handling/usage in biology and for inspiring fabrication of next-generation bio-inspired metallopolymers and adhesives.[24,39,52]

Experimental

Sample preparation

Mytilus edulis mussels supplied from Prince Edward Island, Canada, were raised in a 20 L aquarium with artificial seawater (3%, Fluval Sea, USA). Mussel feet were dissected out and frozen immediately in optimal cutting temperature (OCT) medium and the byssus removed at the stem. Feet samples were stored at

Published on 16 Phata 2024. Downloaded on 2025-12-06 11:36:09.

−80 °C prior to cryo-sectioning with a Leica CM1520 cryo-microtome (Leica, Germany) at −25 °C into 10 μm sections for Raman spectroscopy. For metal-loading experiments, mussels (all between 5–7 cm in size, existing byssus removed) were kept three specimens at a time in 2 L aquaria filled with oxygenated artificial seawater (3%, Fluval Sea, USA) with added micron-sized vanadium (Sigma-Aldrich, USA, CAS 7440-62-2) or iron powder (Thermo Scientific, USA, CAS 7439-89-6) at a concentration of 2 ppm for 24 hours. Specimens were then moved to a 20 L aquarium with artificial seawater and no added metals, adjusted to 15 °C for 72 hours, after which mussel feet would be dissected and any byssus produced in that timeframe removed and rinsed with distilled water for X-ray absorption spectroscopy and ICP-MS analysis.

ICP-MS analysis of V, Fe, Zn concentration

Mussels from V-exposed conditions and native conditions were separately rinsed with distilled water and the foot and byssus were dissected out, rinsed with distilled water, and placed in 5 mL Eppendorf tubes to be lyophilized overnight (Labconco, USA). Once lyophilized, their dry weights were recorded, and samples were digested with Optima Grade concentrated nitric acid (Thermo Scientific, USA, CAS 7697-37-2) and 30% H_2O_2 (Thermo Scientific, USA, CAS 7722-84-1). Samples were digested in acid-cleaned Teflon digestion vessels at room temperature overnight, then heated to 70 °C for four hours, and subsequently diluted to ∼2% w/w nitric acid. Analyses were run in triplicate on each sample using a Finnigan iCapQ ICP-MS (Thermo Scientific, USA), and each sample group consisted of between 2–3 byssi or mussel feet from each condition.

Confocal Raman microscopy and statistical analysis

Raman spectra were collected using a confocal Raman microscope (Alpha 300R, Oxford Instruments, UK) with an excitation wavelength of 532 nm. Spectra were acquired at a magnification of 100× (Zeiss, numerical aperture = 0.9) and a laser power of 3 mW was used for all mapping measurements. These 2D image scans were performed using the instrument's True-Surface capability, collecting 3 spectra per micrometer with a dwell time of 5 s per spectrum. A CCD detector was used to collect scattered light behind a 600-g mm^{-1} grating with a spectral resolution of 4 cm^{-1}. Spectra and images were collected and processed using WITec's ControlFIVE and ProjectFIVE software respectively.

DFT simulated vibrational spectra

To help assign the observed Raman bands, density functional theory implemented on Gaussian16, B3LYP functionals were used with cc-pvdz, and cc-pvtz, basis sets. Vibrational modes were calculated for the cc-pvdz basis sets and the resulting optimized ground states used for the cc-pvtz optimizations and final frequency and activity calculations. All metric and spectroscopic data presented correspond to local gas phase minima with all positive vibrational frequencies. To estimate the degree of catechol *versus* DOPA shifts for these bands the optimized facial 4-methylcatechol complex $[V(O_2C_6H_3Me)_3]_2^-$ was also calculated and the small shifts indicated in Table S5 in the ESI.† Complete lists of all vibrational modes for the $[M(cat)_3]^{n-}$ for both iron and vanadium are also included in the ESI.†

XAS sample preparation and data acquisition

Dry whole byssal threads were mounted on Kapton tape for X-ray absorption analysis. XAS measurements were obtained at the 4-BM (XFM) beamline of the NSLS II synchrotron at Brookhaven National Laboratory (New York, USA) using a Si(111) double crystal monochromator. The ring current was kept at ∼400 mA for the duration of the measurements and spectra were acquired under ambient atmosphere at room temperature in fluorescence geometry, with i_0 and i_t signals measured before and after the sample respectively using ion chambers. The beam spot size was approximately 7 μm across and the fluorescence signal was collected using an energy-dispersive Canberra SXD 7-element Si drift detector (SDD) (Mirion Technologies, USA). XAS spectra were measured at the vanadium Kα edge of 5465 eV to a maximum energy of 350 eV above the edge. Energy step size varied with a maximum energy resolution of 0.25 eV in the pre-edge and near-post-edge regions. The total dwell time for each scan was 15 minutes. One spectrum was acquired per location chosen on the sample, for a total of at least three scans which were then averaged, after verification that no beam-induced photo-reduction was taking place.

Fitting of the EXAFS data

Spectra were aligned with a vanadium foil reference using the ATHENA code of the Demeter software package (version 0.9.26, Ravel and Newville, 2005[53]). E_0 values were chosen as the first peak of the first derivative of spectra in energy space. The data was Fourier-transformed with a weighting of k^2 using a Hanning window and the EXAFS region was fitted within the *R*-range of 1–2.6 Å using the ARTEMIS code, with phases and amplitudes of scattering paths simulated using FEFF6 integrated in ARTEMIS. ${S_0}^2$ was determined by fitting the foil reference in the same manner and was held constant for fitting of the byssal cuticle and plaque spectra. Single scattering V–O paths were used for the fitting procedure based on a V–tris–catecholate reported by Raymond *et al.*[54] It was found that fitting with six identical paths gave a better fit (*R*-factor, reduced chi squared) than fitting with $V–O_{ax}$ and $V–O_{eq}$ paths separately.

Preparation of PEG–DOPA–Fe and PEG–DOPA–V gels (catechol/metal molar ratio 3 : 1) pH = 8

PEG–DOPA was synthesized based on the protocol of Huang *et al.* with minor modifications.[55] Both gels were prepared using a previously reported method with minor adjustments.[56] For each gel, 200 μL of 200 mg mL^{-1} PEG–DOPA was mixed with 66 μL of VCl_3 or $FeCl_3$ (80 mM). Metal salts were in the anhydrous form. At this low pH, both metals form mono coordination complexes with the catechol groups. To induce gelation, 48 μL of 1 M NaOH was added to the mixture raising the pH to ∼8.

 This journal is © The Royal Society of Chemistry and the Centre National de la Recherche Scientifique 2024

Published on 16 Phata 2024. Downloaded on 2025-12-06 11:36:09.

The gels were allowed to relax for 15 minutes before immediately undergoing rheological characterization.

Rheology measurements

Frequency sweep measurements were conducted using a stress-controlled rheometer (MCR 302, Anton Paar) with a 15 mm diameter cone plate measuring system at 1% strain. Peltier temperature control unit was used to control the temperature of the samples and a solvent trap was used to prevent evaporation.

Data availability

The data supporting this article have been included as part of the ESI.†

Conflicts of interest

There are no conflicts to declare.

Acknowledgements

We thank R. Tappero and T. Victor at the 4-BM (XFM) beamline at NSLS-II (Brookhaven National Labs) for technical support and G. Merino and N. Singh for their assistance with the XAS measurements. We thank A. Jung at the Earth and Planetary Sciences ICP-MS facility at McGill for support. We thank F. Jehle for providing an SEM image of the byssus plaque and C. Schmitt for providing Raman spectra of *M. californianus* and *M. galloprovincialis* byssus. This work was supported by the Natural Sciences and Engineering Research Council of Canada (NSERC Discovery Grant RGPIN-2018-05243 for MJH, NSERC Discovery Grant RGPIN-2019-005470 for DSB) and Canada Research Chair awards (CRC Tier 2 950-231953 for MJH, CRC Tier 1 204366 for DSB). SJ was funded by a NSERC PGS D and a FRQNT doctoral training scholarship. TP was funded partially by a FRQNT Quebec Merit Fellowship for Foreign Students.

References

1 C. N. Z. Schmitt, A. Winter, L. Bertinetti, A. Masic, P. Strauch and M. J. Harrington, *J. R. Soc., Interface*, 2015, **12**, 20150466.
2 M. J. Harrington, A. Masic, N. Holten-Andersen, J. H. Waite and P. Fratzl, *Science*, 2010, **328**, 216–220.
3 N. Holten-Andersen, T. E. Mates, M. S. Toprak, G. D. Stucky, F. W. Zok and J. H. Waite, *Langmuir*, 2009, **25**, 3323–3326.
4 J. C. Amiard, C. Amiard-Triquet, S. Barka, J. Pellerin and P. S. Rainbow, *Aquat. Toxicol.*, 2006, **76**, 160–202.
5 C. Guitart, A. Hernández-del-Valle, J. M. Marín and J. Benedicto, *Environ. Sci. Technol.*, 2012, **46**, 11515–11523.
6 D. J. H. Phillips, *Mar. Biol.*, 1976, **38**, 59–69.
7 T. L. Coombs and P. J. Keller, *Aquat. Toxicol.*, 1981, **1**, 291–300.
8 S. G. George, B. J. S. Pirie and T. L. Coombs, *J. Exp. Mar. Biol. Ecol.*, 1976, **23**, 71–84.
9 P. Miramand, J. C. Guary and S. W. Fowler, *Mar. Biol.*, 1980, **56**, 281–293.
10 R. Stefanelli, M. R. Beccia, P. L. Solari, D. Suhard, S. Pagnotta, A. Jeanson, J. U. Mullot, F. Vernier, C. Moulin, M. Monfort, J. Aupiais and C. Den Auwer, *Environ. Res.*, 2024, **252**, 118877.
11 J. C. Amiard, R. Journel and H. Bacheley, *Comp. Biochem. Physiol., Part C: Toxicol. Pharmacol.*, 2008, **147**, 378–385.
12 J. Edel and E. Sabbioni, *Sci. Total Environ.*, 1993, **133**, 139–151.
13 Y. D. Latouche and M. C. Mix, *Mar. Pollut. Bull.*, 1982, **13**, 27–29.
14 T. Priemel, G. Palia, F. Forste, F. Jehle, S. Sviben, I. Mantouvalou, P. Zaslansky, L. Bertinetti and M. J. Harrington, *Science*, 2021, **374**, 206–211.
15 F. Jehle, E. Macías-Sánchez, P. Fratzl, L. Bertinetti and M. J. Harrington, *Nat. Commun.*, 2020, **11**, 862.
16 M. Mesko, L. Xiang, D. S. Bohle, D. S. Hwang, H. B. Zeng and M. J. Harrington, *Chem. Mater.*, 2021, **33**, 6530–6540.
17 J. W. Farrington, B. W. Tripp, S. Tanabe, A. Subramanian, J. L. Sericano, T. L. Wade and A. H. Knap, *Mar. Pollut. Bull.*, 2016, **110**, 501–510.
18 C. N. Z. Schmitt, Y. Politi, A. Reinecke and M. J. Harrington, *Biomacromolecules*, 2015, **16**, 2852–2861.
19 H. B. Zeng, D. S. Hwang, J. N. Israelachvili and J. H. Waite, *Proc. Natl. Acad. Sci. U. S. A.*, 2010, **107**, 12850–12853.
20 D. S. Hwang, H. B. Zeng, A. Masic, M. J. Harrington, J. N. Israelachvili and J. H. Waite, *J. Biol. Chem.*, 2010, **285**, 25850–25858.
21 D. C. Crans, J. J. Smee, E. Gaidamauskas and L. Q. Yang, *Chem. Rev.*, 2004, **104**, 849–902.
22 A. Butler and C. J. Carrano, *Coord. Chem. Rev.*, 1991, **109**, 61–105.
23 D. Rehder, *Metallomics*, 2015, **7**, 730–742.
24 B. P. Lee, P. B. Messersmith, J. N. Israelachvili and J. H. Waite, *Annu. Rev. Mater. Res.*, 2011, **41**, 99–132.
25 E. Khare, N. Holten-Andersen and M. J. Buehler, *Nat. Rev. Mater.*, 2021, **6**, 421–436.
26 I. Michaud-Soret, K. K. Andersson and L. Que, *Biochemistry*, 1995, **34**, 5504–5510.
27 N. Holten-Andersen, A. Jaishankar, M. J. Harrington, D. E. Fullenkamp, G. DiMarco, L. H. He, G. H. McKinley, P. B. Messersmith and K. Y. C. Lee, *J. Mater. Chem. B*, 2014, **2**, 2467–2472.
28 T. Priemel, R. Palia, M. Babych, C. J. Thibodeaux, S. Bourgault and M. J. Harrington, *Proc. Natl. Acad. Sci. U. S. A.*, 2020, **117**, 7613–7621.
29 F. D. Hardcastle and I. E. Wachs, *J. Phys. Chem.*, 1991, **95**, 5031–5041.
30 N. A. Hamada, C. Gilpin and J. J. Wilker, *Environ. Sci. Technol.*, 2020, **54**, 10254–10260.
31 M. Newville, *X-ray Absorption Data Library*, **https://xaslib.xrayabsorption.org/**.
32 M. A. Duchesne, J. Nakano, Y. F. Hu, A. MacLennan, R. W. Hughes, J. Bennett and A. Nakano, *Advances in Molten Slags, Fluxes, and Salts*, 2016, pp. 1405–1412.

Published on 16 Phata 2024. Downloaded on 2025-12-06 11:36:09.

33 J. P. Gustaffson, *Appl. Geochem.*, 2019, **102**, 1–25.
34 P. Frank, K. Kustin, W. E. Robinson, L. Linebaugh and K. O. Hodgson, *Inorg. Chem.*, 1995, **34**, 5942–5949.
35 L. O. Brillouin, *Science and information theory*, Dover Publications, 1956.
36 S. Calvin, *XAFS for Everyone*, Taylor & Francis, 2013.
37 R. K. Bose, N. Hohlbein, S. J. Garcia, A. M. Schmidt and S. van der Zwaag, *Phys. Chem. Chem. Phys.*, 2015, **17**, 1697–1704.
38 W. C. Yount, D. M. Loveless and S. L. Craig, *Angew. Chem., Int. Ed.*, 2005, **44**, 2746–2748.
39 E. Khare, C. G. Obeso, Z. Martín-Moldes, A. Talib, D. L. Kaplan, N. Holten-Andersen, K. G. Blank and M. J. Buehler, *ACS Biomater. Sci. Eng.*, 2024, **10**, 2945–2955.
40 W. X. Sun, B. Xue, Q. Y. Fan, R. H. Tao, C. X. Wang, X. Wang, Y. R. Li, M. Qin, W. Wang, B. Chen and Y. Cao, *Sci. Adv.*, 2020, **6**, eaaz9531.
41 N. Holten-Andersen, M. J. Harrington, H. Birkedal, B. P. Lee, P. B. Messersmith, K. Y. C. Lee and J. H. Waite, *Proc. Natl. Acad. Sci. U. S. A.*, 2011, **108**, 2651–2655.
42 J. P. Park, I. T. Song, J. Lee, J. H. Ryu, Y. Lee and H. Lee, *Chem. Mater.*, 2015, **27**, 105–111.
43 T. Ueki and T. K. Adi, *International Conference on Biology and Applied Science (Icobas)*, 2019, p. 2120.
44 T. Ueki, N. Yamaguchi, R. Romaidi, Y. Isago and H. Tanahashi, *Coord. Chem. Rev.*, 2015, **301**, 300–308.
45 M. Henze, *Biol. Chem.*, 1911, **72**, 494–501.
46 H. Michibata, *Zool. Sci.*, 1996, **13**, 489–502.
47 E. C. Theil and K. N. Raymond, in *Bioinorganic Chemistry*, ed. I. Bertini, University Science Books, Mill Valley, California, 1994, ch. 1.
48 J. C. Pessoa, E. Garribba, M. F. A. Santos and T. Santos-Silva, *Coord. Chem. Rev.*, 2015, **301**, 49–86.
49 T. B. Karpishin, T. D. P. Stack and K. N. Raymond, *J. Am. Chem. Soc.*, 1993, **115**, 182–192.
50 J. H. Waite and M. J. Harrington, *Can. J. Chem.*, 2021, **100**, 197–211.
51 S. A. Adediran and R. F. Pratt, *Biochemistry*, 2008, **47**, 9467–9474.
52 C. H. Li and J. L. Zuo, *Adv. Mater.*, 2020, **32**, 1903762.
53 B. Ravel and M. Newville, *J. Synchrotron Radiat.*, 2005, **12**, 537–541.
54 S. R. Cooper, Y. B. Koh and K. N. Raymond, *J. Am. Chem. Soc.*, 1982, **104**, 5092–5102.
55 W. C. Huang, F. Ali, J. S. Zhao, K. Rhee, C. C. Mou and C. J. Bettinger, *Biomacromolecules*, 2017, **18**, 1162–1171.
56 Q. C. Li, D. G. Barret, P. B. Messersmith and N. Holten-Andersen, *ACS Nano*, 2016, **10**, 1317–1324.

 This journal is © The Royal Society of Chemistry and the Centre National de la Recherche Scientifique 2024